Single-Step Nanoplasmonic VEGF$_{165}$ Aptasensor for Early Cancer Diagnosis

Hansang Cho,[†,‡] Erh-Chia Yeh,[†] Raghu Sinha,[§] Ted A. Laurence,[‡] Jane P. Bearinger,[‡] and Luke P. Lee[†,*]

[†]Berkeley Sensor and Actuator Center, Department of Bioengineering, Department of Electrical Engineering and Computer Science, University of California, Berkeley, California 94720, United States, [‡]Physical and Life Sciences Directorate, Lawrence Livermore National Laboratory, Livermore, California 94550, United States, and [§]Penn State Hershey Cancer Institute, Department of Biochemistry and Molecular Biology, Pennsylvania State College of Medicine, Hershey, Pennsylvania 17033, United States

ABSTRACT

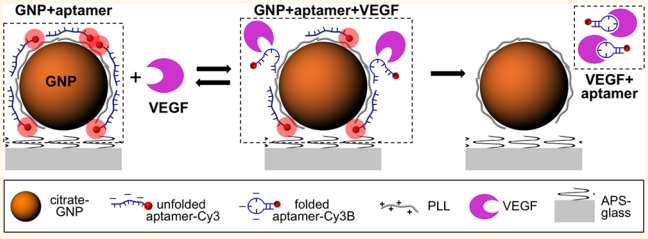

Early cancer diagnosis is very important for the prevention or mitigation of metastasis. However, effective and efficient methods are needed to improve the diagnosis and assessment of cancer. Here, we report a single-step detection method using a nanoplasmonic aptamer sensor (aptasensor), targeting a vascular endothelial growth factor-165 (VEGF$_{165}$), a predominant biomarker of cancer angiogenesis. Our single-step detection is accomplished by (1) specific target recognition by an aptamer—target molecule interaction and (2) direct readouts of the target recognition. The readout is achieved by inactivation of surface plasmon enhancement of fluorescent probes preattached to the aptamers. Our aptasensor provides the appropriate sensitivity for clinical diagnostics with a wide range of linear detection from 25 pg/mL to 25 μg/mL (=from 1.25 pM to 1.25 μM), high specificity for VEGF$_{165}$ against PDGF-BB, osteopontin (OPN), VEGF$_{121}$, NaCl, and temporal/thermal/biological stability. In experiments with 100% serum and saliva from clinical samples, readouts of the aptasensor and an ELISA for VEGF$_{165}$ show good agreement within the limit of the ELISA kit. We envision that our developed aptasensor holds utilities for point-of-care cancer prognostics by incorporating simplicity in detection, low-cost for test, and required small sample volumes.

KEYWORDS: aptamer · surface plasmonic resonance · optical biosensor · VEGF · early cancer diagnostics · prognostics · point-of-care diagnostics

Current cancer diagnostics mainly rely on commercialized multistep antibody-based binding assays, such as, ELISA (enzyme-linked immunosorbent assay),[1,2] Luminex,[3] and Nanosphere[4] for capturing and monitoring target proteins. However, the antibody-based methods require large sample volumes, expensive reagents, or a multistep assay with associated long incubation times. Furthermore, antibody affinity varies from batch to batch, which makes it difficult to develop reliable sensors for clinical molecular diagnostics.

In contrast, aptamers, short single-stranded oligonucleotides (RNA or DNA < 100 nt) or peptides (<100-mer) can be produced through a reliable chemical synthesis.[5,6] Aptamers have high affinity, specificity, and stability; therefore, they are regarded as alternative reagents to antibodies.[7,8] Furthermore, aptamers change structures from an elongated metastable structure to an uniquely folded stable structure upon interaction with targets.[9−11] Such structural change affords monitoring of target-binding events without additional labeling steps.

Recently, numerous aptamer-based biosensors (aptasensors or aptamer beacons)[12] have exploited the target-binding affinity of aptamers and binding-induced conformational changes in aptamers to monitor the interaction with targets by measuring electron transfer,[13−17] color change,[18−22] or fluorescence quenching.[23−30] However, these methods are limited by either the sensor size or sensitivity or by the associated assay complexity. For example, electrochemical sensors designed to measure an electron transfer require electrodes on a millimeter scale to achieve sufficient sensitivity and colorimetric or fluorescence quenching methods require collecting a large amount of particles to induce a discernible color change or fluorescent signals. A previously reported surface-enhanced Raman scattering (SERS) aptasensor required multiple binding events: a sandwich assay requiring labeling of target molecules with the complex of gold nanoparticle/aptamer/Raman probe/silver nanoparticle after capturing the target.[31] Lastly, highly sensitive aptasensors based on surface plasma resonance,[32−34] surface-enhanced resonance Raman scattering (SERRS),[35] and a graphene field-emit transistor (FET)[36] required expensive instruments for measurement, spectral analysis, and sensor fabrication, which limited their extended applications.

In this paper, we present a single-step aptamer-based surface-enhanced fluorescent

* Phone: (510) 642-5855. Fax: (510) 642-5835. Address correspondence to lplee@berkeley.edu.

Received for review October 5, 2011 and accepted August 12, 2012.

Published online August 13, 2012
10.1021/nn203833d

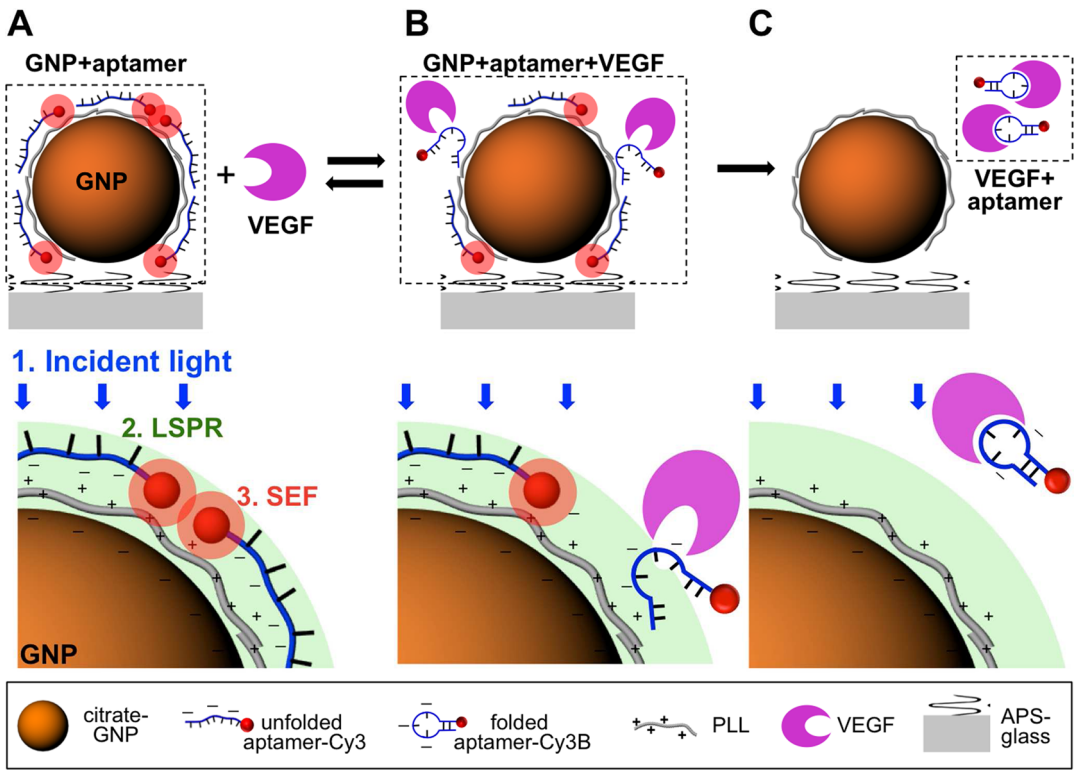

Figure 1. Schematic representations of detection mechanism of the aptasensor for $VEGF_{165}$. (A) In the absence of target molecules, $VEGF_{165}$, unfolded $VEGF_{165}$ aptamer is electrostatically bound to a positively charged PLL-coated gold nanoparticle (GNP) surface and surface-enhanced fluorescence (SEF) of Cy3B conjugated with the $VEGF_{165}$ aptamer is created by both a metal interaction increasing the radiative fluorescent decay rate of Cy3B and the local surface plasmon resonance (LSPR) enhancing the intensity of an incident light. (B) The interaction of the $VEGF_{165}$ aptamer to its target induces the reversible conformation change of the aptamer and, consequently, the decreased electrostatic binding force. (C) As a result, the target-binding interaction of the aptamer causes the irreversible detachment of the aptamer from the GNP surface and avoids the SEF effect of Cy3B.

optical sensor, by combining an aptamer–target interaction for target recognition and a nanoplasmonic–fluorophore interaction for signal enhancement.[37–40] The developed aptasensor is simple, sensitive, specific, and stable for the detection of vascular endothelial growth factor-165 ($VEGF_{165}$), a predominant cancer biomarker in cancer angiogenesis.[41–48]

RESULTS AND DISCUSSION

Strong metal–fluorophore interactions affect the fluorescent intensity significantly. The decay rate of fluorescence increases or decreases depending on the distance from metallic surfaces while the radiative rate in free solution remain relatively constant. The dipole of the fluorophore interacts with free electrons on the metal surface, changing the intensity and temporal and spatial distribution of the radiation. The localization of fluorophores near metal nanoparticles can result in high emission even from "nonfluorescent" molecules and million-fold increases in the number of photons enabling dramatic fluorescent signal enhancement on the nanometer scale.

To implement the metal–fluorophore interaction, negatively charged, citrate-stabilized gold nanoplasmonic particles (GNPs) are fixed on a positively charged aminosilane coated glass slide. On top of GNPs, positively charged poly-L-lysine (PLL) is applied to attract aptamers and stabilize them *via* an electrostatic binding interaction. Additionally, the PLL layer serves as a spacing layer to avoid any quenching effects, which may result from a fluorophore in close proximity to metal. To directly monitor a target binding event without requiring an additional labeling step, the $VEGF_{165}$-specific aptamer is conjugated with a fluorescent molecule, Cy3B, which has an absorption peak wavelength (λ = 552 nm) that matches with a localized surface plasmon resonance (LSPR) peak wavelength of a spherical GNP with 80 nm in diameter ($\lambda \approx 550$ nm),[49] expecting an additional signal enhancement.

Aptamer detachment upon target binding is understood by considering a thermodynamic balance between an aptamer folding energy and an electrostatic binding energy to a PLL-coated surface. Gibbs free energy, ΔG ($=\Delta H - \Delta S$) is considered to quantify proteins or peptides folding in general thermodynamics. In our case, the detachment of the aptamer provides an example of enthalpy and entropy terms competing with one another to determine if an aptamer folding and detachment is a spontaneous process. As in protein folding, the entropic change of the

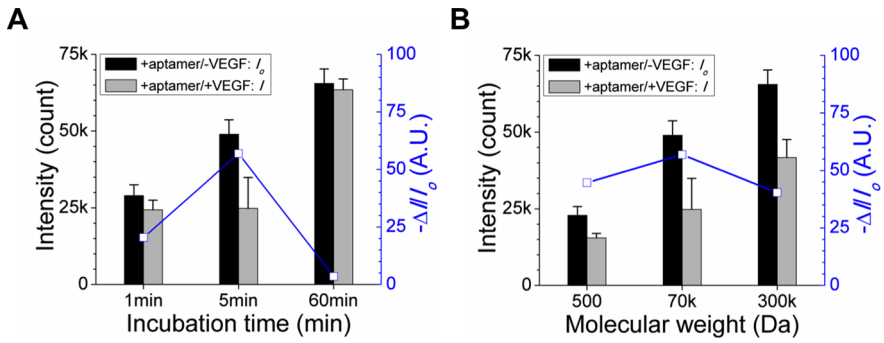

Figure 2. PLL immobilization to improve the signal sensitivity. While the fluorescent intensity of Cy3B in the absence of the target increase with the increase of the molecular weight and the incubation time of PLL, the performance of aptasensor, the normalized intensity change of Cy3B with a target is maximized at around the molecular weight of 70 kDa and the incubation time of 5 min. I and I_0 represent fluorescent intensities from aptasensors in a target solution and treated only with PBS, respectively. ΔI represents the intensity change ($=I - I_0$) by target recognition.

aptamer and the enthalpic contributions are negative with a heat release upon the folding. Analogous to larger proteins, when all of these entropic and enthalpic contributions are combined, the enthalpy term wins out over the entropy term, the free energy of aptamer folding is negative, and aptamer folding can be a spontaneous process.[50] Therefore, we concentrate on the enthalpy term to calculate the aptamer folding energy and compare with the electrostatic binding energy based on calorimetry in an adiabatic condition.

In the absence of a target molecule, it is designed that an electrostatic binding potential, ΔH_E, is of greater magnitude than a spontaneous folding potential, ΔH_S: $0 > \Delta H_S > \Delta H_E$, and the aptamer remains attached to the PLL layer. In this case, Cy3B is spaced at a relevant coupling distance from the GNP surface for the LSPR to induce surface enhanced fluorescence (SEF; Figure 1A). However, the electrostatic potential can be overcome with an addition target-binding folding potential, ΔH_T, which induces a preferable folded structure (Figure 1B). In the case that the folding energy is stronger than the electrostatic binding energy, $0 > \Delta H_E > (\Delta H_S + \Delta H_T)$, the aptamer undergoes a conformational change causing the aptamer to contribute less to the immobilization. The loss of the electrostatic energy leads to the subsequent detachment of aptamers from the GNP surface and signal enhancement is precluded (Figure 1C). Therefore, the concentration of $VEGF_{165}$ molecules can be estimated by measuring the signal change in the fluorescence intensity upon addition of samples.

The spontaneous folding enthalpy of our sequences was calculated to be -66.3 kcal·mol^{-1} (UNAFold, IDT Inc., Coralville, U.S.A.). The electrostatic binding enthalpy was estimated to be -78.2 kcal.mol^{-1} from an experimental measurement.[51] Based on the experimental results from the reference, the additional transitional enthalpy of their sequences due to a combined PLL of 70 kDa was measured to be -3.4 ($=(7.6-14.4)/2$) kcal·mol^{-1}·base pairs^{-1} on average. Based on the measurement, the binding energy of our 23-base sequences was calculated to be -78.2 kcal·mol^{-1}, and consequently, the binding energy to the target was estimated to be of greater magnitude than -11.9 kcal·mol^{-1}.

Signal enhancement by the metal−fluorophore interaction was experimentally confirmed by observing the intensity increase of Cy3B by 33% and the radiative decay rate increase by 24% in the presence of GNPs from a fluorescence lifetime spectroscopic measurement (see Supporting Information, Figure S1).[52] The simultaneous increase in both the intensity and the decay rate could be only enhanced by the metal−fluorophore interaction, while an enhanced light mediated by LSPR could enhance only the intensity and a quenching effect could increase the decay rate but decrease intensity.

The condition of PLL immobilization was determined at an incubation time of 5 min and with 70 kDa molecular weight of PLL that produced the highest signal sensitivity, the ratio of signal change, ΔI, to control signal in the buffer, I_0, among the conditions we considered (Figure 2). As for the application to other cancer markers, with given values of the spontaneous and target-binding folding energies, the electrostatic binding energy can be tailored to be from 0 to -6.8 ($=7.6-14.4$) kcal·mol^{-1}·base pairs^{-1} by varying the molecular weight of a linear PLL and the incubation time of aptamer during aptasensor preparation.[53]

The kinetics of the aptasensor for $VEGF_{165}$ reveals that the signal change reaches saturation within 30 min at 25 ng/mL and about 1 h at 25 pg/mL (Figure 3). Based on the kinetic study covering the physiological concentration of $VEGF_{165}$ in biofluids, all target assays were conducted for an hour. Aptasensors were prepared in an array format fitting to cheaper portable fluorescent scanners for low-cost and simple detection, which was confined by a poly(dimethyl-siloxane) (PDMS) membrane stencil to a silanized glass slide, as shown in Supporting Information, Figure S2. Measured fluorescent signal changes were normalized by the value of the control.

The sensitivity of the aptasensor was evaluated using serially diluted $VEGF_{165}$ solutions in PBS at pH

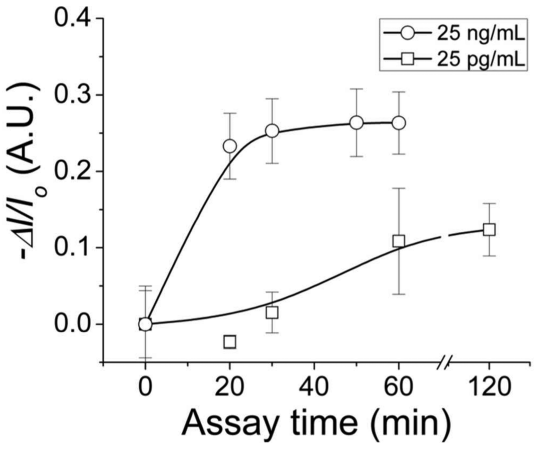

Figure 3. Kinetics of the aptasensor for $VEGF_{165}$. (A) The aptasensor for $VEGF_{165}$ shows that the signal change increases with time and reaches its saturation value within an hour at a concentration from 25 pg/mL to 25 ng/mL, which covers the physiological ranges of $VEGF_{165}$ in clinical samples.

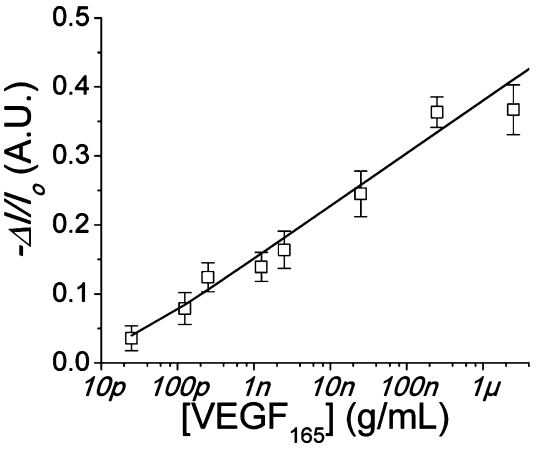

Figure 4. Sensitivity of the aptasensor for $VEGF_{165}$. The aptasensor provides a wide range of detection from 25 pg/mL to 25 μg/mL. The signal changes are linearly proportional to the concentration of $VEGF_{165}$ in a log scale.

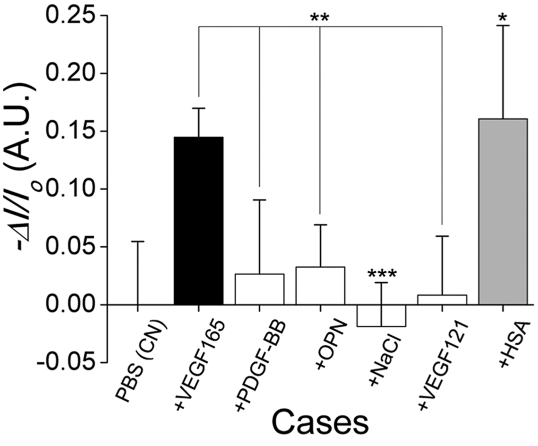

Figure 5. Specificity of the aptasensor for $VEGF_{165}$. The aptasensor has the high specificity with $VEGF_{165}$ against PDGF-BB, OPN (osteopontin), NaCl, and $VEGF_{121}$, but the weak specificity against HSA (human serum albumin). The concentrations of molecules are physiologically relevant values: 2.5 ng/mL ($VEGF_{165}$, PDGF-BB), 1.5 μg/mL (OPN), 560 pg/mL ($VEGF_{121}$), and 40 mg/mL (HSA), excluding an extreme value of 1 M (NaCl). The cases marked with "*", "", and "***" correspond to the assays at nominal, peak, and extreme values present in serum or plasma samples.**

7.4 (Figure 4). The signal changes were proportional to the concentration of $VEGF_{165}$ over a wide range from 25 pg/mL to 25 μg/mL (=from 1.25 pM to 1.25 μM). Based on the averaged values of experiments, the concentration of $VEGF_{165}$ was estimated using the following equation: $[VEGF_{165}] = \exp\{(-\Delta I/I_0 + 0.839)/0.033\} - 1.03e^{-11}$. Average and standard error were calculated with values from four assays.

The aptasensor produced a significant signal change with $VEGF_{165}$ at 2.5 ng/mL, a peak value of breast cancer samples.[37,54] For comparison, signal changes from other cancer-related protein concentrations were not significant as follows: platelet-derived growth factor (PDGF)-BB at 2.5 ng/mL[2] and osteopontin (OPN) at 1.5 μg/mL, the peak values of breast cancer samples[55] and noncancer-related common molecules, NaCl at 1 M, an extremely high value, and $VEGF_{121}$ at 560 pg/mL, a peak value in healthy donors[44,54] (Figure 5). However, the correlation with the most abundant nonspecific protein, HSA, at the average value of 40 mg/mL[56] was discernible. Average and standard error were calculated with values from three assays.

Our sensing mechanism counts on molecular interactions rather than isoelectric potentials of target molecules. Originally, we were concerned with false-positive signaling if a negatively charged aptamer would be replaced by other biomolecules mostly having nonzero isoelectric potentials at pH 7.4. Based on the observation of our results, the electrostatic binding energy of the aptamer seemed to be strong enough against the isoelectric potential of proteins we tested and no false-positive signals were detected from other proteins, PDGF-BB, OPN, and $VEGF_{121}$, except HSA.

The false-positive signal with HSA was presumably resulted from the aptamer replacement by negatively charged HSA. HSA has a lower isoelectric point (pI = 5.3) than the 7.4 buffer pH, resulting in a net negative charge contrary to the other proteins examined (VEGF of pI 9.22 and PDGF of pI 9.8), which have a net positive charge in the buffer but weaker than the positive charge of PLL ($pK_a = 5$) to detach the net negatively charged aptamer. The negative potential of HSA may be higher than that of the aptamer and replace our aptamer from the positively charged PLL. If this is the case, the aptamer should be more strongly immobilized by adding extra spacer sequences and increasing the electrostatic binding force in the future.

Also, it was a concern that salt ions at high concentration might induce folding of our aptamer by increasing the rigidity and resulting in any false-negative signaling.[57] To confirm that there was no false signal, we did an assay with NaCl, the most common salt in

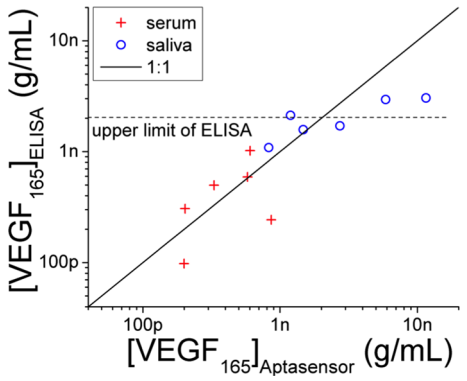

Figure 6. Sensitivity of aptasensor compared with ELISA for $VEGF_{165}$ from clinical samples. The readouts of the aptasensor for $VEGF_{165}$ in undiluted biofluids of serum and saliva from clinical samples are comparable with those of ELISA under 2.0 ng/mL, which is the upper limit of the ELISA kit. Above the limit, the readouts of ELISA are lower than those of aptasensor by several times.

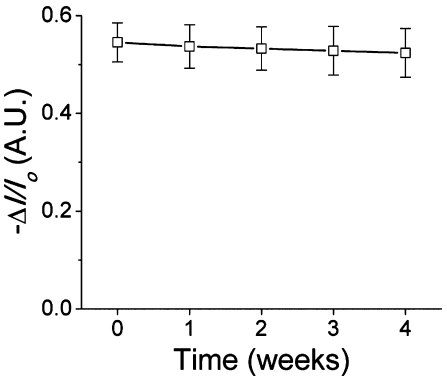

Figure 7. Stability of the aptasensor for $VEGF_{165}$. The temporal stability of fully fabricated aptasensor is evaluated by continually measuring signals from controls of aptasensors in PBS without $VEGF_{165}$ and cases with $VEGF_{165}$ at 20 μg/mL. The signals of control are consistent within the variation range of 5% for a month. The intensity is normalized by the value of a control measured on the first day.

biofluids, at an extremely high concentration to represent the effects from other ions in biofluids. In our experiment, no discernible signal change was observed.

Our developed aptamer-based sensor is regarded to be superior to or comparable with an antibody-based ELISA detection considering its wide detection range and a low cost for testing. A commercial ELISA kit having the detection range from 5 pg/mL to 2 ng/mL can not cover the physiological level of $VEGF_{165}$ in cancer patients (from 500 pg/mL to 8 ng/mL).[44] In the comparative experiments using 100% biofluids of serum and saliva, the detected values of $VEGF_{165}$ with aptasensor matched the values with ELISA under 2 ng/mL, the upper limit of the ELISA kit. Above the limit, the readouts of ELISA was probably saturated and showed lower values than those of aptasensor (Figure 6). The base levels of readouts with aptasensor were elevated in the biofluids probably due to the effect of human serum albumin and the values were calibrated with the obtained sensitivity curve in Figure 4 before the comparison with ELISA.

As provided in the Supporting Information, our aptasensor reagents cost only 7.8¢ per test; the multiwell ELISA kit costs $5.36 per test, partially due to the high cost of antibodies. By mass producing aptasensors and decreasing the sensing area, we can drastically reduce the cost of our aptasensor platform to a price-point well below that of ELISA. In our experiment, we used 10 μL of fabrication agents and samples to cover a sensing area of 7 mm^2, even though an actual detection area was 0.12 mm^2. If we fabricate sensors in the small area, a required volume can be only 170 pL, and, consequently, required agents can be 60 times less in volume and cost.

Our fully fabricated aptasensor was functional after the storage for more than a month at 4 °C (Figure 7). Aptasensors were prepared on individual glass slides at the same time and kept at 4 °C with an aliminium foil cover to prevent any degradation of Cy3B. Every week, slides were chosen for measuring controls of aptasensors in PBS and for experiments on solutions with 20 μg/mL of $VEGF_{165}$. The aptasensor provided consistent signal changes of 50% within a 5% tolerance, showing the temporal stability of aptamers immobilized on GNP surfaces for a month along with thermal stability up to 95 °C provided during sensor preparation and biological stability in biofluids during the assay.

CONCLUSIONS

The single-step aptasensor for $VEGF_{165}$ demonstrated target detection with a small amount of sample solutions (less than 10 μL) within an hour at a low cost (less than 10 ¢/test). In addition, the sensor provided a wide range of linear detection from 25 pg/mL to 25 μg/mL, relevant for clinical diagnostics. Also, the aptasensor of $VEGF_{165}$ detection showed strong specificity against PDGF-BB, OPN, NaCl, and $VEGF_{121}$, and weak specificity against HSA, which could be improved by SELEX works or aptamer modification. Our aptamer-based sensor showed temporal, thermal, and biological stability relevant for harsh diagnostic environments. Furthermore, the performance of aptasensor was successfully validated in biofluids and compared with conventional ELISA.

EXPERIMENTAL SECTION

Materials and Reagents. RNA oligonucleotides were synthesized by IBA GmbH (Göttingen, Germany), purified *via* reverse phase HPLC and confirmed by mass spectroscopy to be >85% pure. The RNA oligonucleotides (23-mer) were fully modified with 2′-O-Me as a VEGF binding aptamer and with Cy3B at 3′

end. A phosphate buffer solution (GIBCO 10010−023) was purchased from Invitrogen (Carlsbad, CA). The sequences of the oligonucleotides[58] and the buffer composition employed in the experiment are as follows: $VEGF_{165}$ binding aptamer (VBA): 5′-ACG CAG UUU GAG AAG UCG CGC GU-3′-Cy3B; 1× PBS: 137 mM NaCl, 2.7 mM KCl, 8 mM Na_2HPO_4, and 2 mM KH_2PO_4 at pH 7.4.

An ELISA kit for $VEGF_{165}$ (Quantikine, DVE00), recombinant human $VEGF_{165}$, $VEGF_{121}$, PDGF-BB, and osteopontin (OPN) were purchased from R&D Systems, Inc. (Minneapolis, MN) and human serum albumin (HSA) was purchased from MP Biomedicals, Inc. (Solon, OH) in a powder form and diluted in sterile PBS to obtain desired stock concentrations. (3-Aminopropyl)triethoxysilane (APS, 98%) and poly-L-lysine (PLL) were purchased from Sigma-Aldrich, Co. (St. Louis, MO). A solution of gold nanoparticles (GNPs, 80 nm in diameter) was purchased from TED Pella, Inc., (Redding, CA) and poly-(dimethyl-siloxane) (PDMS) membrane (HT 6240, 256 μm in thickness) from Rogers Corporation (Woodstock, CT).

Methods. *Preparing Aptasensor.* A glass slide was cleaned with Piranha (3:1 concentrated sulfuric acid to 30% hydrogen peroxide solution) for 10 min, thoroughly washed with DI water, and then dried by a nitrogen gun. After the cleaning, the glass slide was coated with amino-terminal groups by immersing in a diluted APS solution (1% v/v in 100% ethanol) for 5 min at room temperature, rinsing with ethanol, and drying it gently with a nitrogen gun without leaving any trace marks. Baking for 5 min at 125 °C was applied to further stabilize the amino-group layer. Arrayed holes of 3 mm in diameter were patterned on a thin poly(dimethyl-siloxane) (PDMS) membrane (HT 6240) by using the laser-engraving machine (Versa Laser VL-200, Universal Laser Systems, Scottsdale, AZ, U.S.A.). The patterned PDMS membrane was cleaned with ethanol followed by drying with N_2 gas and in an oven at 60 °C for 10 min and then treated with UV/ozone (UVO Cleaner Model 42, Jelight, Irvine, CA) for 3 min to modify the surface of PDMS. GNP stock solution was sonicated (30 s) for even distribution in the stock solution before dropping. A total of 10 μL of the GNP solution was dropped at an opening area defined by the hole on the PDMS membrane and incubated for 1 h at 4 °C in a humidity chamber. Unbound GNPs were washed off by rinsing the slide in distilled water and then drying in a centrifuge (IEC clinical centrifuge, International Equipment Co., Needham, MA). A total of 10 μL of PLL (70k Da M.W., 0.1% in distilled water) was dropped at the opening area and incubated for 5 min at room temperature in the humidity chamber. Unbound PLL was washed off by rinsing the slide in distilled water and then drying in a centrifuge. Aptamers at 500 nM were fully dehybridized and stretched by heating to 90 °C for 2 min in a dry block heater (HeatBlock I, VWR International, LLC, West Chester, PA) above a calculated melting temperature of 64 °C. A 10 μL aliquot of the aptamer solution was dropped immediately at the opening area and incubated for 1 h at 70 °C in the humidity chamber. Unbound aptamers were gently washed off by rinsing the slide in PBS by gently pipetting and then drying in a centrifuge.

Target Assay with Aptasensor. For assay, 10 μL samples (biofluids, $VEGF_{165}$, and other molecules) were dropped at the opening area and incubated for 1 h at room temperature in the humidity chamber. Target-combined aptamers and unbound molecules were washed off by gently pipetting each sensor with 10 μL of PBS while avoiding cross-contamination. Thorough washing induced the nonspecific signal loss due to the unwanted detachment of the aptamers and GNPs by a nonspecific mechanical force.

Target Assay with ELISA. Undiluted human serum and saliva samples were assayed for $VEGF_{165}$ using an ELISA kit according to the manufacturer's instructions. The concentration of $VEGF_{165}$ in these samples was extrapolated from a standard curve generated using a range (0−2 ng/mL) of highly purified *Sf* 21-expressed recombinant human $VEGF_{165}$.

Biofluid Samples. Nonsmoking participants were recruited at the GCRC, Penn State College of Medicine, Hershey, PA, for this study. All the subjects involved in this study signed the institutional review board-approved consent form. As for the comparative assay, clinical samples were prepard with the mixed population of four healthy women with no known breast disease and four women diagnosed as breast cancer ranging from infiltrating ductal carcinoma, ductal carcinoma *in situ*, to invasive cribiform carcinoma, and invasive lobular carcinoma. All of the breast cancer patients were recently diagnosed and had not received any prior treatment in the form of chemotherapy, radiotherapy, surgery, or alternative remedies before sample collection. The mean ages for breast cancer patients and healthy donors were 46.0 ± 9.6 yr and 49.3 ± 5.4 yr ($P > 0.05$, t test), respectively. Fasting blood and stimulated whole saliva samples using base-gum (a gift from Wrigley's) and blood samples were collected. Separated serum and centrifuged saliva samples (12000 rpm for 10 min) were stored at −80 °C until used.

Lifetime Measurement. A home-built sample scanning confocal microscope (TE300, Nikon Instruments Inc., Melville, NY) was equipped with a pulsed diode laser (LDH-P-C-470B, PicoQuant GmbH, Berlin, Germany), 470 nm in wavelength, a time-correlated single photon counting module (PicoHarp 300, Picoquant GmbH, Berlin, Germany), and a piezo scanning stage (Nano-LP 200, Mad City Laboratories Inc., Madison, WI). A fluorescent molecule, Cy3B, conjugated with aptamer was excited by the laser with a power of 2 μW and a pulse rate of 40 MHz. The fluorescence was excited and collected through an oil immersion objective lens (Plan Apochromat, 60×, N/A = 1.4, Nikon), and filtered with a 580 nm bandpass filter (580DF60, Omega Optical Inc., Brattleboro, VT). The photons were detected with an avalanche photodiode (PDM series, Micro Photon Devices, Bolzano, Italy), and the time delay between the laser pulse and the photons was measured using the PicoHarp 300. From each measurement we acquired images for 10 s, performing a line scan over 100 μm. After the measurement, the lifetimes were fitted by a sum of two exponentials, accounting for a measured instrument response. The sum of the two resulting exponential decay rates, weighted by the amplitudes was used to compute the decay rates changes quoted in Figure S1.

Fluorescence Imaging. An inverted microscope (TE2000-E, Nikon Instruments Inc., Melville, NY) was coupled with a mercury lamp (1× HBO 103w/2, OSRAM, München, Germany) and a monochrome CCD camera (Cascade 512B, Photomatrics, Tucson, AZ). The lights were filtered with a TRITC fluorescence filter set (EX: 528−553 nm, DM: 565 nm, BA: 578−633 nm) through an objective lens (Plan Fluor, 20×, N/A = 0.45, Nikon). The fluorescent images of aptasensors were acquired using a commercial program (Image-pro Express, Media Cybernetics, Inc., Bethesda, MD) with an acquisition time of 200 ms and a gain factor of 3 and then stored in a 16-bit depth monochrome image.

Dark Field Imaging. An inverted microscope (Axiovert 200, Carl Zeiss, Göttingen, Germany) was equipped with a white light illumination (Xenon Light Source 610, KARL STORZ GmbH and Co. KG, Tuttlingen, Germany), a wet dark-field condenser (1.2 < NA < 1.4), and a true-color digital camera (MP3.3-RTV-CLR-10, QImaging, Surrey, BC, Canada). Space between arrayed aptasensors and the condenser was filled with PBS and maintained at room temperature in a complete dark room. The true-color images of aptasensors were taken through an objective lens (LD ACHROPLAN, 40×, NA = 0.6, Zeiss), acquired with a commercial program (QCapture Pro, Media Cybernetics, Inc., Bethesda, MD) with an acquisition time of 100 ms and a gain factor of 1, and then stored in a 24-bit true color image.

Conflict of Interest: The authors declare no competing financial interest.

Acknowledgment. The authors acknowledge the funding from LLNL under Contract DE-AC52-07NA27344 (LLNL-JRNL-428054), NIH/NCI Center of Cancer Nanotechnology Excellence (CCNE), and the Center for Nanostructured Materials and Technology (CNMT) under the 21st Century Frontier Research Programs of the Korea government. We thank the GCRC Staff at Penn State College of Medicine for assistance in blood and saliva collection, E. Lee, and J. Park for providing guidance on surface chemistry.

Supporting Information Available: An experimental validation of metal−fluoroscent interaction, photos of an arrayed aptasensor platform, and cost estimation of aptasensor. This material is available free of charge *via* the Internet at http://pubs.acs.org.

REFERENCES AND NOTES

1. Etzioni, R.; Urban, N.; Ramsey, S.; McIntosh, M.; Schwartz, S.; Reid, B.; Radich, J.; Anderson, G.; Hartwell, L. The Case for Early Detection. *Nat. Rev. Cancer* **2003**, *3*, 243–252.
2. Rifai, N.; Gillette, M. A.; Carr, S. A. Protein Biomarker Discovery and Validation: The Long and Uncertain Path to Clinical Utility. *Nat. Biotechnol.* **2006**, *24*, 971–983.
3. Albani, S.; Prakken, B.; Cell Epitope−Specific, T Immune Therapy for Rheumatic Diseases. *Arthritis Rheum.* **2006**, *54*, 19–25.
4. Park, S.-J.; Taton, T. A.; Mirkin, C. A. Array-Based Electrical Detection of DNA with Nanoparticle Probes. *Science* **2002**, *295*, 1503–1506.
5. Ellington, A. D.; Szostak, J. W. *In Vitro* Selection of RNA Molecules that Bind Specific Ligands. *Nature* **1990**, *346*, 818–822.
6. Tuerk, C.; Gold, L. Systematic Evolution of Ligands by Exponential Enrichment: RNA Ligands to Bacteriophage T4 DNA Polymerase. *Science* **1990**, *249*, 505–510.
7. Cho, E. J.; Lee, J.-W.; Ellington, A. D. Applications of Aptamers as Sensors. *Annu. Rev. Anal. Chem.* **2009**, *2*, 241–264.
8. Nguyen, T.; Hilton, J.; Lin, Q. Emerging Applications of Aptamers to Micro- and Nanoscale Biosensing. *Microfluid. Nanofluid.* **2009**, *6*, 347–362.
9. Bock, L. C.; Griffin, L. C.; Latham, J. A.; Vermaas, E. H.; Toole, J. J. Selection of Single-Stranded DNA Molecules that Bind and Inhibit Human Thrombin. *Nature* **1992**, *355*, 564–566.
10. Baker, B. R.; Lai, R. Y.; Wood, M. S.; Doctor, E. H.; Heeger, A. J.; Plaxco, K. W. An Electronic, Aptamer-Based Small-Molecule Sensor for the Rapid, Label-Free Detection of Cocaine in Adulterated Samples and Biological Fluids. *J. Am. Chem. Soc.* **2006**, *128*, 3138–3139.
11. Sefah, K.; Phillips, J. A.; Xiong, X.; Meng, L.; Van Simaeys, D.; Chen, H.; Martin, J.; Tan, W. Nucleic Acid Aptamers for Biosensors and Bio-Analytical Applications. *Analyst* **2009**, *134*, 1765–1775.
12. Levy, M.; Cater, S. F.; Ellington, A. D. Quantum-Dot Aptamer Beacons for the Detection of Proteins. *ChemBioChem* **2005**, *6*, 2163–2166.
13. Zheng, G.; Patolsky, F.; Cui, Y.; Wang, W. U.; Lieber, C. M. Multiplexed Electrical Detection of Cancer Markers with Nanowire Sensor Arrays. *Nat. Biotechnol.* **2005**, *23*, 1294–1301.
14. Swensen, J. S.; Xiao, Y.; Ferguson, B. S.; Lubin, A. A.; Lai, R. Y.; Heeger, A. J.; Plaxco, K. W.; Soh, H. T. Continuous, Real-Time Monitoring of Cocaine in Undiluted Blood Serum *via* a Microfluidic, Electrochemical Aptamer-Based Sensor. *J. Am. Chem. Soc.* **2009**, *131*, 4262–4266.
15. Zhao, S.; Yang, W.; Lai, R. Y. A Folding-Based Electrochemical Aptasensor for Detection of Vascular Endothelial Growth Factor in Human Whole Blood. *Biosens. Bioelectron.* **2011**, *26*, 2442–2447.
16. Xiao, Y.; Lubin, A. A.; Heeger, A. J.; Plaxco, K. W. Label-Free Electronic Detection of Thrombin in Blood Serum by Using an Aptamer-Based Sensor. *Angew. Chem., Int. Ed.* **2005**, *44*, 5456–5459.
17. Zhao, J.; He, X.; Bo, B.; Liu, X.; Yin, Y.; Li, G. A "Signal-On" Electrochemical Aptasensor for Simultaneous Detection of Two Tumor Markers. *Biosens. Bioelectron.* **2012**, *34*, 249–252.
18. Yang, C. J.; Jockusch, S.; Vicens, M.; Turro, N. J.; Tan, W. Light-Switching Excimer Probes for Rapid Protein Monitoring in Complex Biological Fluids. *Proc. Natl. Acad. Sci. U.S.A.* **2005**, *102*, 17278–17283.
19. Huang, C. C.; Huang, Y. F.; Cao, Z.; Tan, W.; Chang, H. T. Aptamer-Modified Gold Nanoparticles for Colorimetric Determination of Platelet-Derived Growth Factors and their Receptors. *Anal. Chem.* **2005**, *77*, 5735–5741.
20. Lu, W.; Arumugam, S. R.; Senapati, D.; Singh, A. K.; Arbneshi, T.; Khan, S. A.; Yu, H.; Ray, P. C. Multifunctional Oval-Shaped Gold-Nanoparticle-Based Selective Detection of Breast Cancer Cells Using Simple Colorimetric and Highly Sensitive Two-Photon Scattering Assay. *ACS Nano* **2010**, *4*, 1739–1749.
21. Waldeisen, J. R.; Wang, T.; Ross, B. M.; Lee, L. P. Disassembly of a Core-Satellite Nanoassembled Substrate for Colorimetric Biomolecular Detection. *ACS Nano* **2011**, *5*, 5383–5389.
22. Shukoor, M. I.; Altman, M. O.; Han, D.; Bayrac, A. T.; Ocsoy, I.; Zhu, Z.; Tan, W. Aptamer-Nanoparticle Assembly for Logic-Based Detection. *ACS Appl. Mater. Interfaces* **2012**, *4*, 3007–3011.
23. Lee, H.; Sun, E.; Ham, D.; Weissleder, R. Chip-NMR Biosensor for Detection and Molecular Analysis of Cells. *Nat. Med.* **2008**, *14*, 869–874.
24. Galanzha, E. I.; Shashkov, E. V.; Kelly, T.; Kim, J.-W.; Yang, L.; Zharov, V. P. *In Vivo* Magnetic Enrichment and Multiplex Photoacoustic Detection of Circulating Tumour Cells. *Nat. Nanotechnol.* **2009**, *4*, 855–860.
25. Nielsen, L. J.; Olsen, L. F.; Ozalp, V. C. Aptamers Embedded in Polyacrylamide Nanoparticles: a Tool for *In Vivo* Metabolite Sensing. *ACS Nano* **2010**, *4*, 4361–4370.
26. Freeman, R.; Liu, X.; Willner, I. Chemiluminescent and Chemiluminescence Resonance Energy Transfer (CRET) Detection of DNA, Metal Ions, and Aptamer−Substrate Complexes Using Hemin/G-Quadruplexes and CdSe/ZnS Quantum Dots. *J. Am. Chem. Soc.* **2011**, *133*, 11597–11604.
27. Yang, Y.; Zhao, L. Sensitive Fluorescent Sensing for DNA Assay. *TrAC Trends Anal. Chem.* **2010**, *29*, 980–1003.
28. Jiang, G.; Susha, A. S.; Lutich, A. A.; Stefani, F. D.; Feldmann, J.; Rogach, A. L. Cascaded FRET in Conjugated Polymer/Quantum Dot/Dye-Labeled DNA Complexes for DNA Hybridization Detection. *ACS Nano* **2009**, *3*, 4127–4131.
29. Wang, Y.; Bao, L.; Liu, Z.; Pang, D.-W. Aptamer Biosensor Based on Fluorescence Resonance Energy Transfer from Upconverting Phosphors to Carbon Nanoparticles for Thrombin Detection in Human Plasma. *Anal. Chem.* **2011**, *83*, 8130–8137.
30. Freeman, R.; Girsh, J.; Fang-ju Jou, A.; Ho, J.-a. A.; Hug, T.; Dernedde, J.; Willner, I. Optical Aptasensors for the Analysis of the Vascular Endothelial Growth Factor (VEGF). *Anal. Chem.* **2012**, *84*, 6192–6198.
31. Wang, Y.; Wei, H.; Li, B.; Ren, W.; Guo, S.; Dong, S.; Wang, E. SERS Opens a New Way in Aptasensor for Protein Recognition with High Sensitivity and Selectivity. *Chem. Commun.* **2007**, 5220–5222.
32. Li, Y.; Lee, H. J.; Corn, R. M. Detection of Protein Biomarkers Using RNA Aptamer Microarrays and Enzymatically Amplified SPR Imaging. *Anal. Chem.* **2007**, *79*, 1082–1088.
33. Kaur, H.; Yung, L. Y. Probing High Affinity Sequences of DNA Aptamer against VEGF(165). *PLoS One* **2012**, *7*, e31196–e31196.
34. Pimková, K.; Bocková, M.; Hegnerová, K.; Suttnar, J.; Čermák, J.; Homola, J.; Dyr, J. Surface Plasmon Resonance Biosensor for the Detection of VEGFR-1: A Protein Marker of Myelodysplastic Syndromes. *Anal. Bioanal. Chem.* **2012**, *402*, 381–387.
35. Cho, H.; Baker, B. R.; Wachsmann-Hogiu, S.; Pagba, C. V.; Laurence, T. A.; Lane, S. M.; Lee, L. P.; Tok, J. B. H. Aptamer-Based SERRS Sensor for Thrombin Detection. *Nano Lett.* **2008**, *8*, 4386–4390.
36. Kwon, O. S.; Park, S. J.; Hong, J.-Y.; Han, A. R.; Lee, J. S.; Lee, J. S.; Oh, J. H.; Jang, J. Flexible FET-Type VEGF Aptasensor Based on Nitrogen-Doped Graphene Converted from Conducting Polymer. *ACS Nano* **2012**, *6*, 1486–1493.
37. Lakowicz, J. R. Radiative Decay Engineering: Biophysical and Biomedical Applications. *Anal. Biochem.* **2001**, *298*, 1–24.
38. Zhang, J.; Malicka, J.; Gryczynski, I.; Lakowicz, J. R. Surface-Enhanced Fluorescence of Fluorescein-Labeled Oligonucleotides Capped on Silver Nanoparticles. *J. Phys. Chem. B* **2005**, *109*, 7643–7648.
39. Ray, K.; Zhang, J.; Lakowicz, J. R. Fluorescence Lifetime Correlation Spectroscopic Study of Fluorophore-Labeled Silver Nanoparticles. *Anal. Chem.* **2008**, *80*, 7313–7318.
40. Kang, K. A; Wang, J.; Jasinski, J. B; Achilefu, S. Fluorescence Manipulation by Gold Nanoparticles: From Complete Quenching to Extensive Enhancement. *J. Nanobiotechnol.* **2011**, *9*, article no. 16.

41. Homer, J. J.; Anyanwu, K.; Ell, S. R.; Greenman, J.; Stafford, N. D. Serum Vascular Endothelial Growth Factor in Patients with Head and Neck Squamous Cell Carcinoma. *Clin. Otolaryngol. Allied Sci.* **1999**, *24*, 426–430.
42. Bogin, L.; Degani, H. Hormonal Regulation of VEGF in Orthotopic MCF7 Human Breast Cancer. *Cancer Res.* **2002**, *62*, 1948–1951.
43. Kim, E. S.; Serur, A.; Huang, J.; Manley, C. A.; McCrudden, K. W.; Frischer, J. S.; Soffer, S. Z.; Ring, L.; New, T.; Zabski, S.; et al. Potent VEGF Blockade Causes Regression of Coopted Vessels in a Model of Neuroblastoma. *Proc. Natl. Acad. Sci. U.S.A.* **2002**, *99*, 11399–11404.
44. Brattström, D.; Bergqvist, M.; Hesselius, P.; Larsson, A.; Wagenius, G.; Brodin, O. Serum VEGF and bFGF Adds Prognostic Information in Patients with Normal Platelet Counts When Sampled before, during and after Treatment for Locally Advanced Non-Small Cell Lung Cancer. *Lung Cancer* **2004**, *43*, 55–62.
45. Ferrara, N. Vascular Endothelial Growth Factor: Basic Science and Clinical Progress. *Endocrinol. Rev.* **2004**, *25*, 581–611.
46. Ng, E. W. M.; Shima, D. T.; Calias, P.; Cunningham, E. T.; Guyer, D. R.; Adamis, A. P. Pegaptanib, a Targeted Anti-VEGF Aptamer for Ocular Vascular Disease. *Nat. Rev. Drug Discovery* **2006**, *5*, 123–132.
47. Nishijima, K.; Ng, Y.-S.; Zhong, L.; Bradley, J.; Schubert, W.; Jo, N.; Akita, J.; Samuelsson, S. J.; Robinson, G. S.; Adamis, A. P.; et al. Vascular Endothelial Growth Factor-A Is a Survival Factor for Retinal Neurons and a Critical Neuroprotectant during the Adaptive Response to Ischemic Injury. *Am. J. Pathol.* **2007**, *171*, 53–67.
48. Zhu, A. X.; Duda, D. G.; Sahani, D. V.; Jain, R. K. HCC and Angiogenesis: Possible Targets and Future Directions. *Nat. Rev. Clin. Oncol.* **2011**, *8*, 292–301.
49. Mie, G. Beiträge zur Optik Trüber Medien, Speziell Kolloidaler Metallösungen. *Ann. Phys.* **1908**, *330*, 377–445.
50. Pratt, C. W.; Cornely, K. *Essential Biochemistry*; John Wiley and Sons: Hoboken, NJ, 2004.
51. H, K. Calorimetric Studies of the Interaction between DNA and Poly-L-lysine. *Biophys. Chem.* **1976**, *5*, 363–367.
52. Laurence, T. A.; Chromy, B. Efficient Maximum Likelihood Estimator Fitting of Histograms. *Nat. Methods* **2010**, *7*, 338–339.
53. Männistö, M.; Vanderkerken, S.; Toncheva, V.; Elomaa, M.; Ruponen, M.; Schacht, E.; Urtti, A. Structure–Activity Relationships of Poly(L-lysines): Effects of Pegylation and Molecular Shape on Physicochemical and Biological Properties in Gene Delivery. *J. Controlled Release* **2002**, *83*, 169–182.
54. Adams, J.; Carder, P. J.; Downey, S.; Forbes, M. A.; MacLennan, K.; Allgar, V.; Kaufman, S.; Hallam, S.; Bicknell, R.; Walker, J. J.; et al. Vascular Endothelial Growth Factor (VEGF) in Breast Cancer: Comparison of Plasma, Serum, and Tissue VEGF and Microvessel Density and Effects of Tamoxifen. *Cancer Res.* **2000**, *60*, 2898–2905.
55. Tuck, A. B.; Chambers, A. F. The Role of Osteopontin in Breast Cancer: Clinical and Experimental Studies. *J. Mammary Gland Biol. Neoplasia* **2001**, *6*, 419–429.
56. Carter, D. C.; Ho, J. X. Structure of Serum Albumin. *Adv. Protein Chem.* **1994**, *45*, 153–203.
57. McIntosh, D. B.; Saleh, O. A. Salt Species-Dependent Electrostatic Effects on ssDNA Elasticity. *Macromolecules* **2011**, *44*, 2328–2333.
58. Burmeister, P. E.; Lewis, S. D.; Silva, R. F.; Preiss, J. R.; Horwitz, L. R.; Pendergrast, P. S.; McCauley, T. G.; Kurz, J. C.; Epstein, D. M.; Wilson, C.; et al. Direct *In Vitro* Selection of a 2′-O-Methyl Aptamer to VEGF. *Chem. Biol.* **2005**, *12*, 25–33.